Food Hydrocolloids 83 (2018) 36–44

Contents lists available at ScienceDirect

Food Hydrocolloids

journal homepage: www.elsevier.com/locate/foodhyd

Protection of astaxanthin from photodegradation by its inclusion in hierarchically assembled nano and microstructures with potential as food

Carlos Alarcón-Alarcón [a, 1], Mariela Inostroza-Riquelme [a, b, 1], César Torres-Gallegos [a, c], Claudio Araya [d], Miguel Miranda [e], Juan Carlos Sánchez-Caamaño [e], Ignacio Moreno-Villoslada [a, *], Felipe A. Oyarzun-Ampuero [b, **]

[a] Instituto de Ciencias Químicas, Facultad de Ciencias, Universidad Austral de Chile, Las Encinas 220, Valdivia, Chile
[b] Departamento de Ciencias y Tecnología Farmacéuticas, Facultad de Ciencias Químicas y Farmacéuticas, Universidad de Chile, Santos Dumont 964, Santiago, Chile
[c] Programa de Doctorado en Ciencias de la Acuicultura, Universidad Austral de Chile, Los Pinos s/n, Balneario Pelluco, Puerto Montt, Chile
[d] Laboratorio de Biología del Desarrollo, Instituto de Ciencias Marinas y Limnológicas, Facultad de Ciencias, Universidad Austral Chile, Las Encinas 220, Valdivia, Chile
[e] Estación Experimental Quillaipe, Fundación Chile, Kilómetro 25, Carretera Austral, Puerto Montt, Chile

ARTICLE INFO

Article history:
Received 1 August 2017
Received in revised form
12 April 2018
Accepted 16 April 2018
Available online 19 April 2018

Keywords:
Astaxanthin
Nanosystems
Chitosan hydrogels
Alginate beads
Food
Photodegradation

ABSTRACT

Astaxanthin is a light sensitive molecule which is already approved as a dietary supplement, with a wide range of biological properties in humans and fishes. In this paper, we provide strategies to photostabilize the pigment through its inclusion in easy-to-prepare and scale up formulations, comprising non-toxic excipients. Astaxanthin has been formulated in biocompatible hierarchically assembled structures in order to produce model food to humans and fishes. The structures present increasing complexity in the following order: 1) oily nanodroplets stabilized by phospholipids; 2) chitosan-coated nanoemulsions produced after coating the nanodroplets with chitosan; 3) carrageenan-coated nanoemulsions produced after coating chitosan-coated nanoemulsions with carrageenan; 4) calcium alginate and chitosan tripolyphosphate beads including one of the nanosystems. The sensitivity to UV light of astaxanthin in both the nanosystems and the hydrogels has been evaluated. The nanoformulations produce protection of astaxanthin from photodegradation in the order nanoemulsions > carrageenan-coated nanoemulsions > chitosan-coated nanoemulsions. Chitosan beads furnish higher protection to astaxanthin than alginate beads. In a preliminary assay in fishes, alginate beads of 2–3 mm and 160 μm containing the nutrient were supplied to adult *Danio rerio* and juvenile *Eleginops maclovinus*, respectively. Both living species showed high rates of capturing the hydrogels in the water column, corroborating the attractiveness of the formulations as food for fishes. Due to the easy preparation of the formulations (that exclude thermal treatment or the use of toxic solvents), and the flexibility of these hierarchically assembled materials to incorporate other active molecules (proteins, polyunsaturated fatty acids, oligoelements, oral vaccines, antibiotics, antiparasitic, etc.), we postulate these formulations as ideal platforms to create foods for humans and animal species.

1. Introduction

Astaxanthin (3,3′-dihydroxy-β-carotene-4,4′-dione, AST) is a lipophilic carotenoid widely used in the food industry (Gammone, Riccioni, & D'Orazio, 2015; Shah, Liang, Cheng, & Daroch, 2016). AST is already approved as a dietary supplement and is widely available commercially (Grimmig, Kim, Nash, Bickford, & Douglas Shytle, 2017). Among broad biological activities of this supplement we

* Corresponding author.
** Corresponding author.
E-mail addresses: imorenovilloslada@uach.cl (I. Moreno-Villoslada), foyarzuna@ciq.uchile.cl (F.A. Oyarzun-Ampuero).
[1] Both authors contributed equally to this work.

https://doi.org/10.1016/j.foodhyd.2018.04.033
0268-005X/

can underline benefits in cardiovascular health, metabolic syndrome, treatment of gastric ulcers, and cancer, all of which have elements of inflammation and/or oxidative stress (Ambati, Phang, Ravi, & Aswathanarayana, 2014). In fishes, it also demonstrated an important role in the sexual maturity, increasing fertility and egg survival (Amar, Kiron, Satoh, & Watanabe, 2001; Higuera-Ciapara, Felix-Valenzuela, & Goycoolea, 2006; Nakano, Tosa, & Takeuchi, 1995). Its presence in diets for salmons strongly impacts their growth and survival rates (Christiansen, Lie, & Torrissen, 1995). Importantly, it is the responsible for the orange-red color of salmon meat, a parameter of great importance in the industry. Astaxanthin has an extended conjugated structure, highly reactive in the presence of free radicals and reactive oxygen species such as singlet oxygen (Kobayashi et al., 1997; Kobayashi & Sakamoto, 1999; Naguib, 2000). These characteristics are responsible for its general antioxidant functionality and protective action against oxidative damage in cells, trapping and stabilizing free radicals and avoiding radical reactions with essential cell components such as DNA, proteins, membranes, mitochondria, etc. Related with its antioxidant properties, AST is easily degraded by thermal, oxidative, and photo-oxidative processes, which lead to inactivation of the molecule, losing functional, organoleptic, and nutritional properties (Sweeney & Marsh, 1973). It is important, therefore, to avoid these factors during food processing that limits the optimum integration of astaxanthin into a food matrix (Gouveia & Empis, 2003).

Encapsulation in the food industry may afford protection from moisture, heat, or other extreme conditions, thus enhancing stability and durability (Gibbs, Kermasha, Alli, & Mulligan, 1999; Nedovic, Kalusevic, Manojlovic, Levic, & Bugarski, 2011; Shahidi & Han, 1993). Hierarchically assembled structures allow, by means of providing different coatings, controlling the stability and diffusion kinetics of encapsulated molecules making use of their physicochemical properties, such as lipophilia and specific binding interactions. Among the different techniques to encapsulate molecules, nanometric sized structures such as nanoemulsions and nanocapsules, and micro and macrometric architectures such as hydrogel beads are found. The ability of a variety of polymers to form hydrogels has been widely described in the state of the art. Due to their capacity to respond to environmental pH and ionic strength, polyelectrolyte polymers represent very promising excipients to create hydrogels. Elaboration of hydrogels comprising polyelectrolyte gels involves, in many cases, mixing aqueous fluids containing oppositely charged macromolecules (complexation) or macromolecules with oppositely charged ions (gelation) (Hassan et al., 2014). Importantly, production of such hydrogels proceeds in mild conditions, in most cases without involving thermal treatment, thus avoiding damage of sensitive nutrients such as polyunsaturated fatty acids and proteins or peptides. Importantly, antioxidant molecules (Higuera-Ciapara, Felix-Valenzuela, Goycoolea, & Argüelles-Monal, 2004), vaccines (Li et al., 2008), prebiotics and probiotics (Chávarri et al., 2010; Krasaekoopt, Bhandari, & Deeth, 2006) may be easily included in such hydrogels preserving their physical and chemical integrity. Among widely used spherical hydrogels we find calcium alginate beads and chitosan tripolyphosphate beads. Both formulations are based on polysaccharides, ionically cross-linked, thus avoiding the formation of covalent bonds through chemical reactions that may jeopardize biocompatibility. Alginate is a polyanionic species, while chitosan is polycationic.

Due to its hydrophobicity, a uniform distribution of AST in polysaccharide beads is highly limited since the molecule can not be directly dissolved or dispersed in the hydrogel medium (Rivas-Aravena, Sandino, & Spencer, 2013). The incorporation of such hydrophobic low molecular-weight species in higher-order structures, preferably amphiphilic nanosystems, may help their homogenous dispersion and retention (Flores et al., 2016). Nanoemulsions and polymeric coated nanoemulsions are adequate means of incorporation of hydrophobic nutrients approved by food regulatory agencies, such as fatty acids, triglycerides, and pigments (McClements, 2013; Sotomayor-Gerding et al., 2016). Thus, AST may be easily formulated in nanoemulsions stabilized by lecithin, that allows controlling the net charge sign and other phisicalchemical properties by the incorporation of co-surfactants (Orellana, Torres-Gallegos, Araya-Hermosilla, Oyarzun-Ampuero, & Moreno-Villoslada, 2015; Oyarzun-Ampuero, Rivera-Rodríguez, Alonso, & Torres, 2013), and/or polysaccharide coatings (Oyarzun-Ampuero et al., 2013).

In this work, we hypothesize that the inclusion of AST in nanoemulsions and polymeric coated nanoemulsions may be advantageous for its protection against photodegradation. This strategy of formulation could represent other important advantages to AST, such as: a) its release in a controlled manner (Alishahi, Mirvaghefi, Tehrani, Farahmand, Shojaosadati, et al., 2011); b) its easy incorporation in beads able to be consumed by humans and fishes; and c) its improved visual acceptance furnishing the beads with nice color. Thus, we will formulate oil-in-water nanoemulsions and cationic and anionic polymeric coated nanoemulsions (with chitosan and carrageenan coatings, respectively) containing AST, and analyze the rate of photodegradation of the pigment. Additionally, we will study the inclusion of these nanostructures in calcium alginate and chitosan tripolyphosphate beads and analyze the photodegradation of AST, and also the transformation of the beads to a dry powder. Moreover, loaded beads, both at milli- and micrometric size (prepared manually and automatically, respectively) will be given to juvenile (*Eleginops maclovinus*) and adult fishes (*Danio rerio*), in order to preliminary check attractiveness and toxicity.

2. Experimental

2.1. Materials

AST (Astax S.A.-Chile), EPIKURON 145 V lecithin-based mixture of surfactants (Cargill-USA), WAGLINOL 3/9280 caprylic-capric triglyceride mixture (Industrial Química Lasem-Spain), chitosan medium molecular weight (Sigma-Aldrich, USA, 80% deacetylation degree, REF. 448877, 248.4 g/mol of ionizable groups considered), sodium alginate (Sigma-Aldrich, UK, REF. A2158, 198 g/mol of ionizable groups considered), and carrageenan iota type (Gelymar, Chile, 255 g/mol of ionizable groups considered) were used to prepare solutions and materials in deionized water or in ethanol (J.T. Backer, USA) or acetone (Merck, USA). The concentration of the polysaccharides is given in mol of ionizable groups per liter. $CaCl_2$ (Merck, USA) and sodium tripolyphosphate (Sigma-Aldrich, USA) were used as ionic cross-linkers for alginate and chitosan, respectively. The structures of AST and the polysaccharides are shown in Fig. 1. Gemma Wean 0.2 micro-pellets (Skretting, Chile) were used as control food in bioassays.

2.2. Animals

Fishes were used for animal experimentation under the rules of *Fundación Chile* and the *Universidad Austral de Chile*, surveyed by the *Use of Experimental Animals Committee* (DID-UACh). Adult AB wild-type zebrafishes (*Danio rerio*) were kept in 4 L aquaria tanks within a closed recirculation system at 26–28 °C with 14 h/10 h day/night light cycles, 700 μS of conductivity and pH 7.0. Fishes were fed daily with dry food and *Artemia* sp. and fasted for 24 h prior to be fed with polysaccharide beads in the context of the

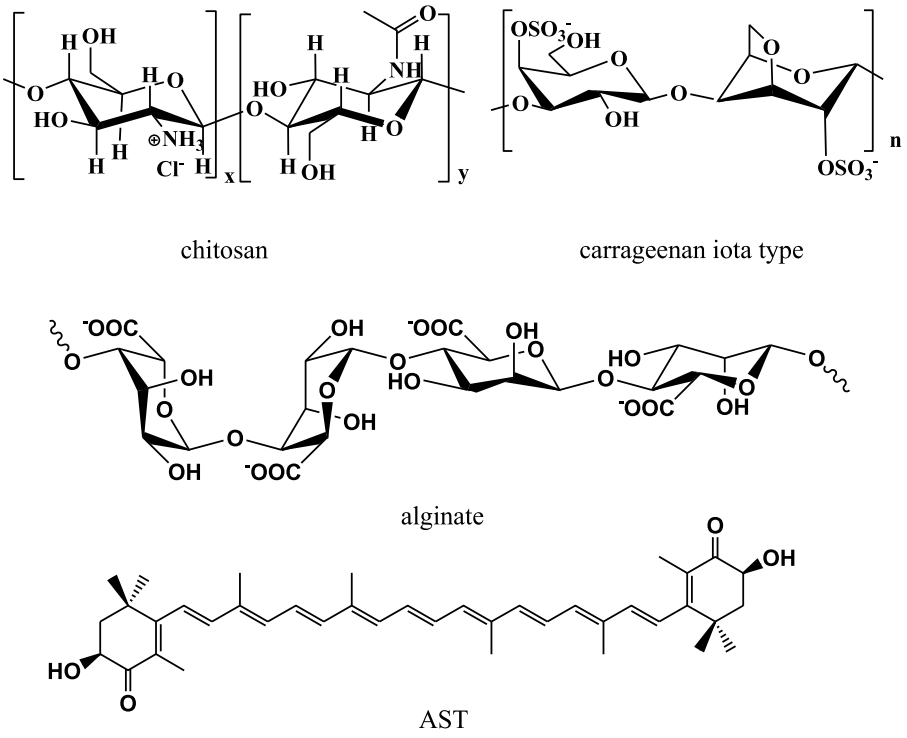

Fig. 1. Molecular structure of the polysaccharides used and AST.

present research. Juvenile snooks (*Eleginops maclovinus*), whose body weight was around 250 mg, were kept in 150 L tanks filled at half capacity with filtered/airy sea water at 14 °C and 14 h/10 h day/night light cycles. The tanks were equipped with a water exchange system allowing continuous aeration of 8 mg/L of oxygen achieving a 96% of oxygen saturation.

2.3. Equipment and analytical methods

Solutions and nanostructures were prepared under stirring with the aid of a JEIO TECH HP 3000 magnetic stirrer. Organic solvents were removed in an IKA RV 10 rotary evaporator. The solution pH was controlled with UB10 DENVER and CORNING Scholar 425 pH meters. Characterization of hydrodynamic diameter, polydispersity index (PDI), and zeta potential of the nanostructures was performed in a Malvern Nano ZS zetasizer fitted with a 633 nm laser (Malvern Instruments, UK). The intensity-averaged particle diameter and the PDI of the nanostructures were determined by dynamic light scattering (DLS) with 173° backscatter detection. The electrophoretic mobility values, measured by laser Doppler velocimetry, were converted to zeta potential by the Smoluchowski equation. Scanning transmission electron microscopy (STEM) analyses were done in an Inspect 50 microscope (FEI-USA). STEM images were obtained by sticking a droplet (10 μL) of the nanoparticle suspension on a copper grid (200 mesh, covered with Formvar) for 2 min, then removing the droplet with filter paper avoiding the paper touching the grid, then washing twice the grid with a droplet of Milli-Q water for 1 min, and removing the droplet with filter paper. Later, the sample was stained with a solution of 1% phosphotungstic acid by sticking a droplet of this solution on the grid for 2 min and removing the droplet with filter paper. Finally, the grid was allowed to dry for at least 1 h before analysis. Photodegradation was induced with a Bio Light lamp (40 W) operating at 254 nm. Optical images were taken with a Nikon D3000 camera. UV-vis analyses were taken in a Heλios γ spectrophotometer (Thermo Scientific). The micrometric hydrogels were elaborated using a B-395 Pro microencapsulator (Büchi) and the size and shape of the microstructures were analyzed using an Olympus CKX41 optical microscope. Dehydration of microsystems was made using a FreeZone 1 freeze-dryer (LABCONCO).

2.4. Procedures

All procedures and analysis have been performed at 25 °C unless other values are specified.

2.4.1. Oil-in-water nanoemulsions preparation

Nanoemulsions were prepared following a procedure similar to previous published works with slight modifications (Orellana et al., 2015; Oyarzun-Ampuero et al., 2013). An organic phase was formed in a test tube by dissolving 30 mg of EPIKURON 145 V in 0.5 mL of ethanol, then adding 125 μL of WAGLINOL, and manually mixing the resulting solution with 10 mL of a 1×10^{-4} M solution of AST in acetone. The organic phase was quickly poured into a flask (50 mL) containing 20 mL of deionized water (aqueous phase) under vigorous stirring during 5 min using a magnetic stirrer. A milky suspension is immediately formed indicating the spontaneous development of the nanoemulsions. The mixture is then concentrated to 10 mL by rotary evaporation (35 °C), removing the organic solvents. Stability in time of the nanosystems was tested at 4 °C.

2.4.2. Chitosan-coated nanoemulsions preparation

Chitosan-coated nanoemulsions were prepared by the same method but, in this case, the aqueous phase consisted of 20 mL of an aqueous solution of chitosan (0.05% w/v, 2×10^{-3} M), prepared by dissolving 10 mg of chitosan in 2 mL of acetic acid 0.1% w/v, and then completing with water to 20 mL.

2.4.3. Carrageenan-coated nanoemulsions preparation

Carrageenan-coated nanoemulsions were prepared incubating for 10 min 4 mL of suspensions of chitosan-coated nanoemulsions in 4 mL of 3×10^{-3} M carrageenan aqueous solution under stirring.

2.4.4. AST photodegradation

3 mL of suspensions of the different nanostructures were placed in quartz vessels of 1×1 cm^2 of base surface, and 3 cm of height, normally used for UV-vis spectroscopic analyses, and placed at 10 cm from the light source operating at 254 nm. The samples were subjected to UV radiation for variable periods of time. After definite time intervals, aliquots of 100 μL of the suspensions were taken and diluted in 900 μL of acetone, and the relative concentration of AST analyzed by UV-vis spectrometry in quartz cuvettes at 480 nm.

2.4.5. Manual macrometric hydrogel preparation

1 mL of a 1.5×10^{-1} M aqueous solution of sodium alginate was mixed in test tubes (during 30 s using a vortex) with 300 μL of a suspension of the corresponding nanosystems. The resulting mixture was poured drop by drop, using a syringe with a 27 G needle to which the end has been cut perpendicular to its main symmetry axis, into a 50 mL precipiated glass containing 10 mL of 0.1 M $CaCl_2$, under magnetic stirring. The same procedure was done with chitosan at a concentration of 7.5×10^{-2} M using TPP at a concentration of 0.1 M as cross-linker.

2.4.6. Hydrogel photodegradation

The formed hydrogels were placed at 6 cm of the light source operating at 254 nm and pictures were taken after definite time intervals.

2.4.7. Automatic micrometric hydrogel preparation

An aqueous solution of sodium alginate mixed with AST nanoemulsion was dripped over the $CaCl_2$ solution (under magnetic stirring) at a rate of 2.3 mL/min controlling the size of the drop with a selected nozzle of 120 μm, and applying a frequency of 6000 Hz and a voltage of 900 V that allowed generating a flux of droplets dispersed in a wide cone. Once the hydrogels are formed and decant at the bottom of the container, the excess of $CaCl_2$ was removed, and the beads washed twice with deionized water.

2.4.8. Hydrogel dehydration

The microsystems suspended in 10 mL of water were frozen using liquid nitrogen (−200 °C), and then water was sublimated in the freeze-dryer during 24 h at −50 °C and 0.11 bar.

2.4.9. Animal assays

2.4.9.1. Adult zebrafish and macrometric beads. Two adult zebrafishes were transferred to a 1 L flask filled with water at 28 °C. Then ≈1 g of manually prepared hydrogels of around 2 mm of diameter containing AST was added dropwise and the consumption was digitally recorded with a Nikon D3000 camera.

2.4.9.2. Juvenile snook and micrometric beads. Three groups of ten individuals of juvenile snook where used in the bioassay. Two groups were fed with prepared calcium alginate microbeads containing AST nanoemulsions, and the third group with control pellets (Gemma Wean 0.2 micro-pellets, Skretting). Each group was immersed in a 150 L tank at half capacity with filtered/airy sea water at 14 °C and equipped with a water exchange system allowing continuous aeration of 8 mg/L of oxygen achieving a 96% of oxygen saturation. Fishes were habituated during three days to the experimental conditions previous to the development of the bioassay that lasted 20 days. Administered dose of the diets (microdiets and control food) corresponded to a 3% of the total biomass of each group and was divided in two daily rations furnished at 9:00 and 16:00 h. The consumption was analyzed indirectly by collecting the residuals of each tank, 2 h after the last administration, and separating the feces from unconsumed diet. Then the collected microdiets and control food were weighed and compared with the administered mass of each diet, thus obtaining an approach of food uptake. The specific growth rate (SGR) was analyzed after the 20 days bioassay period following the equation:

$$SGR = \ln(\text{final biomass} / \text{initial biomass}) / \text{time} \quad (1)$$

3. Results and discussion

3.1. Formation and characterization of the nanosystems containing AST

Anionic nanoemulsions were prepared by pouring the organic phase containing AST into water. The obtained nanoemulsions presented nanodroplets of hydrodynamic diameter in the range of 150–160 nm of diameter, showing a low PDI ranging between of 0.086 and 0.108, and a negative zeta potential ranging between −27 and −55 mV (n = 4), comparing different batches. The negative charge of the nanodroplets is responsible for the stability of the nanosuspension. The stability of the formulation in aqueous medium at 4 °C corresponding to a single batch has been analyzed during a lapse of 18 days, and the results are shown in Fig. 2A, error bars corresponding to the different measurements for a single batch (n = 3). It can be observed that the hydrodynamic diameter of the nanodroplets is conserved, and the zeta potential remains in the negative part of the scale, lower than −20 mV, considered as a threshold beyond which the nanoemulsions lose stability. The formation of the nanosystems has been also corroborated by STEM analyses, as can be seen in Fig. 3A, where nanostructures of spherical appearance are seen.

Chitosan-coated nanoemulsions were prepared by pouring the organic phase containing AST into a chitosan aqueous solution. Due to that chitosan and some surfactants in the EPIKURON 145 V mixture are sensitive to the pH, the pH was adjusted to different values. The results concerning the hydrodynamic diameter and zeta potential of the formed coated nanoemulsions are shown in Table 1. The error values given correspond to the different measurements for a single batch. Values considering different batches at pH 3.5 differ from each other so that the hydrodynamic diameter for the different coated nanoemulsions have been found to range between 218 and 255 nm (n = 3). For the reported batch in Table 1, it can be seen that the chitosan-coated nanoemulsions could be formed at pHs ranging between 2.0 and 3.5, presenting positive zeta potential ranging between +56 and + 71 mV, high enough to ensure stability of the suspensions, and hydrodynamic diameter in the range of 200–350 nm, with differences that may not be consider significant when comparing different batches. The PDI values were also small (≤0.3), corresponding to monomodal size distributions. At higher pHs, the mixtures undergo phase separation in the form of macroscopic precipitates. The lower charge of chitosan achieved upon deprotonation and the higher negative charge of the surfactants containing carboxylic units may be responsible for a drop down on the zeta potential upon neutralization, with consequent destabilization of the emulsion. The stability of chitosan-coated nanoemulsions prepared at pH 3.5 has also been studied during 18 days at 4 °C, as can be seen in Fig. 2B. It is observed that the formulations resulted stable in this period of time, and both hydrodynamic diameter and zeta potential are conserved under ranges that ensure stability. STEM images also witness the

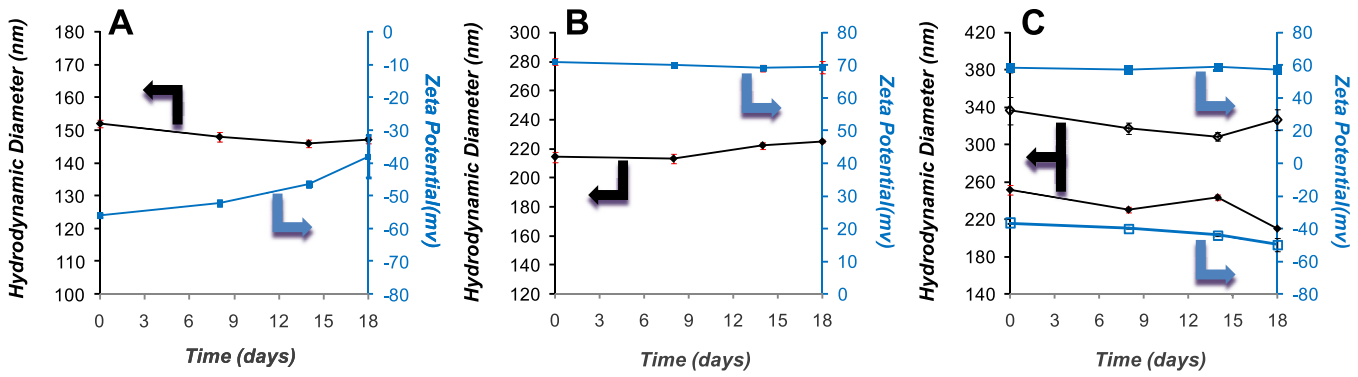

Fig. 2. Apparent hydrodynamic diameter (◆) and zeta potential (■) as a function of time (data and standard deviation, n = 3) of uncoated nanoemulsions (**A**), chitosan-coated nanoemulsions at pH 3.5 (**B**), and carrageenan-coated nanoemulsions obtained incubating chitosan-coated nanoemulsions in carrageenan solutions at concentrations of 1.0×10^{-3} M (filled symbols) and 3.0×10^{-3} M (empty symbols) (C).

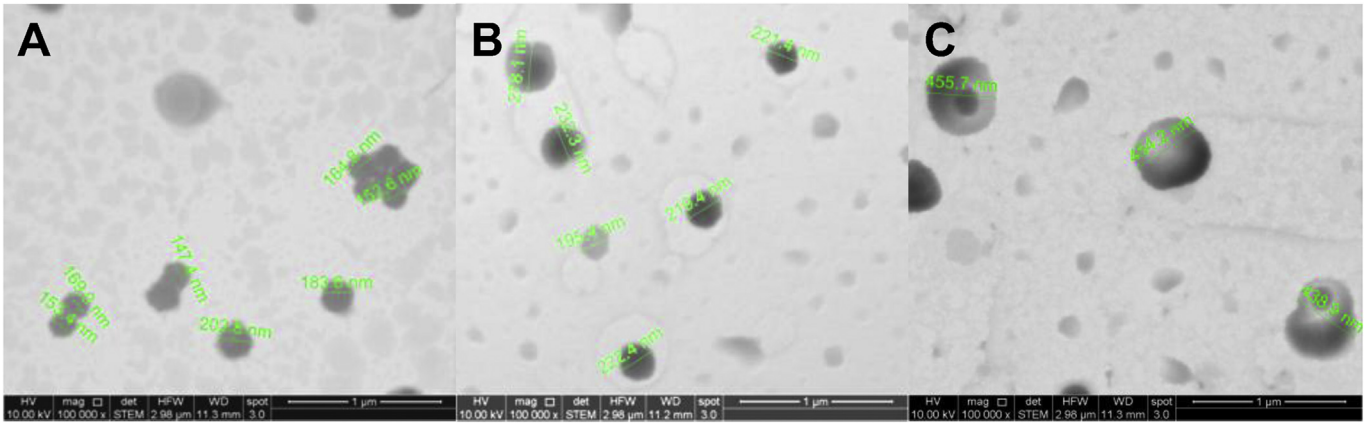

Fig. 3. STEM images of uncoated nanoemulsions (**A**), cationic chitosan-coated nanoemulsions (**B**), and anionic carrageenan-coated nanoemulsions (**C**).

Table 1
Apparent hydrodynamic diameter, PDI, and zeta potential of the cationic chitosan-coated nanoemulsions as a function of the pH (n = 3). *pp* refers to macroprecipitation.

pH	Hydrodynamic diameter (nm)	PDI	Zeta potential (mV)
2.0	325 ± 6.4	0.3	56 ± 2.3
2.5	221 ± 1.2	0.2	64 ± 2.1
3.0	205 ± 2.1	0.2	66 ± 2.0
3.5	241 ± 0.2	0.2	71 ± 1.7
4.0	*pp*	–	–

formation of the coated nanoemulsions (Fig. 3B), showing particles of diameters in the order of magnitude observed in suspension by DLS.

Anionic carrageenan-coated nanoemulsions were prepared by incubation of the cationic chitosan-coated nanoemulsions formed at pH 3.5 in solutions of carrageenan. Carrageenan is expected to coat the cationic chitosan-coated nanoemulsions by electrostatic interactions. Through these interactions, the net charge of the particles necessarily changes. Thus, experiments were performed using carrageenan solutions of different concentrations. The resulting hydrodynamic diameter and zeta potential of the carrageenan-coated nanoemulsions were then analyzed. As can be read in Table 2, at low concentration of the polyanion, the surface charge of the coated nanoemulsions remains positive, due to an excess of chitosan at the interface. Upon increasing the concentration of carrageenan, the net charge decreases up to a limit at which stability, attributed to electrostatic repulsion, is lost, and then its sign changes, with increasing absolute values, providing stability to the nanosystems. Thus, the carrageenan content surpasses that of chitosan in the coatings, creating a net negative charge on the nanodroplet shell. The hydrodynamic diameter of the nanosystems increases as more carrageenan is incorporated. The values given in Table 2 correspond to the different measurements for a single batch. Values considering different batches for coated nanoemulsions containing an amount of carrageenan associated to positive zeta potential showed hydrodynamic diameters ranging between 200 and 420 nm, whereas those associated to negative zeta potential showed hydrodynamic diameters ranging between 340 and 560 nm. The stability of cationic and anionic carrageenan-coated nanoemulsions obtained in one batch was also studied during 18 days at 4 °C (Fig. 2C). Cationic carrageenan-coated nanoemulsions formed at pH 3.5 at a concentration of carrageenan 1×10^{-3} M show stable hydrodynamic diameter ranging between 210 and 250 nm, and stable positive zeta potential ranging between +57 and + 59 mV. On the other hand, good stability was also found for anionic carrageenan-coated nanoemulsions formed at a concentration of carrageenan 3×10^{-3} M, showing hydrodynamic diameter ranging between 310 and 340 nm, and negative zeta potential ranging between −37 and −50 mV. STEM images in Fig. 3C do also show the formation of anionic carrageenan-coated

Table 2
Apparent hydrodynamic diameter, PDI, and zeta potential of carrageenan-coated nanoemulsions as a function of the carrageenan concentration.

Carrageenan concentration (M)	Hydrodynamic diameter (nm)	PDI	Zeta potential (mV)
$0.5 \cdot 10^{-4}$	233 ± 3.7	0.26	65 ± 2.0
$1.0 \cdot 10^{-3}$	265 ± 2.8	0.35	63 ± 0.2
$1.5 \cdot 10^{-3}$	271 ± 3.5	0.41	60 ± 0.2
$2.0 \cdot 10^{-3}$	324 ± 11.3	0.44	59 ± 1.2
$2.5 \cdot 10^{-3}$	–	–	–
$3.0 \cdot 10^{-3}$	445 ± 9.1	0.55	−35 ± 0.2
$3.5 \cdot 10^{-3}$	442 ± 6.2	0.50	−48 ± 0.6
$4.0 \cdot 10^{-3}$	460 ± 11	0.60	−47 ± 0.8

nanoemulsions with higher diameters than their parent anionic uncoated and chitosan-coated nanoemulsions.

AST, free in acetone, and included in aqueous-dispersed nanosystems, was exposed to UV radiation for 500 min. It can be seen in Fig. 4 that the nanosystems protect AST from photodegradation, since the pristine pigment is degraded in the first 130 min, while encapsulated in the nanosystems is not completely degraded in the course of 500 min. However, it can be noticed that the chitosan-coated nanoemulsions provide less resistance to photodegradation to AST than anionic uncoated nanoemulsions or anionic carrageenan-coated nanoemulsions. In particular, the uncoated nanoemulsions produce the best photoresistance. In order to explain the difference on the protective effect of the nanosystems, one must take into consideration that both coated nanoemulsions contain chitosan, a polymer bearing free amino groups that are also photoreactive, forming free radicals that may react with AST (Wasikiewicz, Yoshii, Nagasawa, Wach, & Mitomo, 2005). The presence of carrageenan in the nanosystems may produce protection against photodegradation of chitosan, since ionic interaction makes the free amino groups less reactive.

The photodegradation of AST in the irradiated samples shows kinetics of order one in most cases, witnessed by the decrease on its total apparent concentration in the samples. The logarithm of the AST concentration normalized for the initial value at $t = 0$ (t = time) is plotted in Fig. 5. The kinetic constants can be obtained from the slope of the linear adjustments, and the values found are shown in Table 3. Good correlations are found for every formulation with the exception of the carrageenan-coated nanoemulsions, in which AST shows a higher resistance to be degraded in the first hour, and then loses its resistance ability, so that its concentration quickly drops down (Fig. 5). This can be due to transference mechanisms between radicals involving chitosan and carrageenan up to saturation.

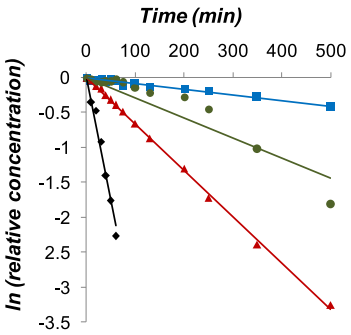

Fig. 5. Logarithm of the normalized concentration of AST as a function of time in: acetone (◆), uncoated nanoemulsions (■), cationic chitosan-coated nanoemulsions (▲), anionic carrageenan-coated nanoemulsions (●).

Table 3
Kinetic constants of photodegradation of AST included in different nanosystems; R^2 is the linear regression factor obtained for the curves plotted in Fig. 5.

System	Kinetic constants (min^{-1})	R^2
AST/acetone	0.0378	0.98
AST/uncoated nanoemulsions	0.00078	0.96
AST/cationic chitosan-coated nanoemulsions	0.00666	1.00
AST/anionic carrageenan-coated nanoemulsions	0.00333	0.88

3.2. Calcium alginate and chitosan tripolyphosphate beads loaded with AST

Low polydisperse spherical calcium alginate and chitosan

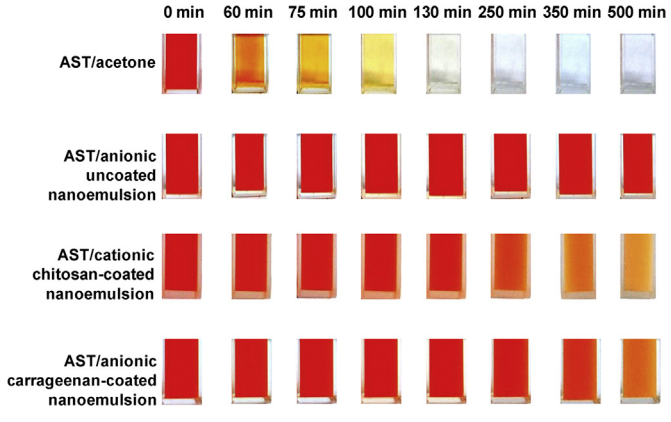

Fig. 4. Photodegradation of AST, free in acetone, and in nanosystems dispersed in water, as a function of time.

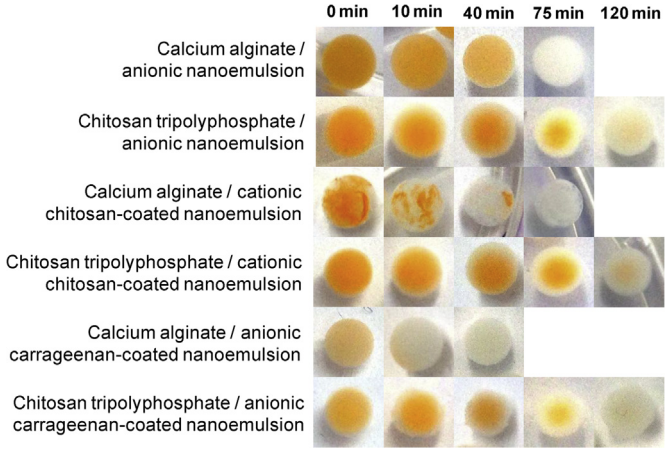

Fig. 6. Photodegradation of AST in polysaccharide beads of 2–3 mm of diameter.

tripolyphosphate beads containing AST were formed by the dripping technique, as can be seen in Fig. 6. The inclusion of the nanostructures helps the formation of very regular beads of similar hydrodynamic diameter, since they change the surface tension of the suspensions. The diameter of the beads ranged between 2 and 3 mm. The formulation of hydrogels containing AST involves the mixture of the synthesized nanostructures with alginate or chitosan polymers prior to cross-linking with Ca^{2+} and TPP, respectively. It could be observed a higher tendency to flocculate when mixing anionic nanostructures with the positively charged polysaccharide chitosan, or the cationic nanostructures with the negatively charged alginate, which is reasonably attributed to ionic incompatibilities between the oppositely charged components. The rest of the systems showed AST homogenously distributed in the hydrogels.

The susceptibility of AST to be photodegraded in these structures has also been studied, and the results are also shown in Fig. 6. As said before, chitosan molecules may form radicals upon irradiation, contributing to the discoloration of AST. The same can be said for alginate, due to its carboxylic groups. It is interesting to observe the different discoloration patterns of the beads considering the different nature of the base polymer. Observed at naked eye, calcium alginate beads were homogenously discolored on their entire volume, while chitosan tripolyphosphate beads appear discolored form outside to inside. Alginate beads appear completely discolored in the lapse of 75 min, and it could be seen that in this case uncoated nanoemulsions protect AST from photodegradation more efficiently, consistent with the results shown in Fig. 4 for nanostructures dispersed in water. On the contrary, the discoloration kinetics of chitosan tripolyphosphate beads, conceived as the decrease on the radius of the colored sphere versus time, presented similar values for the three systems assayed, ranging between 0.005 and 0.007 mm/min. The results are shown in Fig. 7.

3.3. Calcium alginate microbeads loaded with uncoated nanoemulsions containing AST

Microgels can be generated using automatic machinery (Whelehan & Marison, 2011), which in addition facilitates the industrial application of the technology. Nanoemulsions were selected as the nanoformulations to stabilize AST in aqueous media due to their higher photoresistance to degradation. In order to produce calcium alginate microbeads containing AST nanoemulsions, the alginate/nanoemulsion mixture was extruded through a 120 μm of diameter nozzle. Fig. 8A and B shows the developed microformulations suspended in water and analyzed by optical microscopy and at naked eye, respectively, showing spherical microbeads of 161 ± 17 μm. The formation of microgels whose size is larger than the diameter of the used nozzle is commonly described in the literature (Whelehan & Marison, 2011). In order to facilitate the storage, dosage, and administration of the microgels, formulations were freeze-dried generating an orange powder easy to resuspend in water (Fig. 8C).

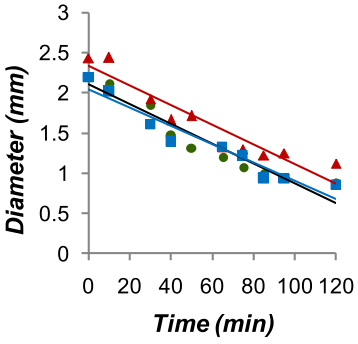

Fig. 7. Diameter of the colored sphere in chitosan tripolyphosphate beads as a function of time containing AST included in uncoated nanoemulsions (■), cationic chitosan-coated nanoemulsions (▲), anionic carrageenan-coated nanoemulsions (●).

3.4. Preliminary assay in fishes

As a proof of concept of the potential of AST to produce visual stimuli to fishes to consume the model food, alginate beads of 2–3 mm of diameter loaded with AST nanoemulsions were administered as diet supply to adult zebrafish in order to verify whether or not the beads were consumed. As it can be appreciated in Video S1 (supporting information), the administered dose (≈1 g) consumption by fishes was complete revealing that beads represent an appetizing food. Due to that juvenile fishes may require food with smaller dimensions, we also proceeded with the administration of micrometric beads loaded with AST nanoemulsions of 160 μm to juvenile snook during 20 days. The micrometric food was previously freeze-dried in order to facilitate its storage and transport to the hatchery. During the 20 days at which the diet was maintained, none of the 20 juvenile fishes died, revealing the safeness of the microformulation. The pellets used as control food presented a mean diameter of 200 μm. As can be read in Table 4, the uptake of the assayed food relative to the initial biomass was in the order of 0.2–0.3 during the 20 days of the assay, and the SGR took values between 0.2 and 0.4%. Although these values are smaller than those obtained with the control food, the attractive properties of the microgels and their non-toxicity are demonstrated with this experiment.

Supplementary video related to this article can be found at https://doi.org/10.1016/j.foodhyd.2018.04.033.

The microgel formulation assayed here is far from representing a final food. However, considering that the microbeads loaded with AST nanoemulsions are prepared without the use of toxic solvents and do not require high temperatures in the elaboration process, its enrichment with a variety of sensitive active molecules (proteins, polyunsaturated fatty acids, oligoelements, oral vaccines, antibiotics, antiparasitic, etc.) is easy, thus showing potential to humans and animal species. Due to the importance of visual factors, beads loaded with the colored AST may be effective to improve visual stimuli (spherical shape and nice color) and ingestion (preventing from strong flavor and smell) of AST. The formulation flexibility of these hierarchically assembled materials, incorporating nanosystems such as nanoemulsions and coated nanoemulsions containing biologically active molecules, allows the load of both hydrophilic and hydrophobic substances. In addition, polyelectrolytes such as chitosan or carrageenan help stimulating beneficial immunogenic responses (Alishahi, Mirvaghefi, Tehrani, Farahmand, Koshio, et al., 2011) and protection from pathogenic microorganisms (Aider, 2010; Valenzuela & Arias, 2012), as well as bear mucoadhesion properties to the formulations that prolong the residence time of the nutrients in the intestine, thus improving absorption and biodisponibility (Grenha et al., 2010; Prabaharan, 2008).

This general property of the hydrogels, the specific properties of AST, and the synergistic action towards protection of AST degradation by light, promotes hydrogels containing AST as ideal platforms to create foods for humans and fishes.

4. Conclusions

The inclusion of AST in nanosystems produces protection from photodegradation in the order nanoemulsions > carrageenan-

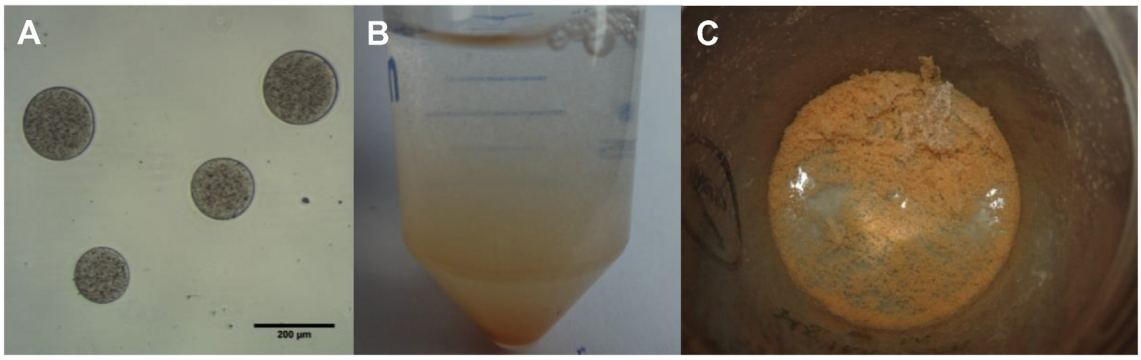

Fig. 8. Images of micrometric alginate beads containing AST uncoated naneomulsions suspended in water obtained by optical microscopy (**A**), at naked eye (**B**), and freeze-dried (**C**).

Table 4
Consumption data and SGR of juvenile snook fed with calcium alginate containing AST nanoemulsions (groups 1 and 2) and control food (group 3). For each group, the number of fishes was 10.

Group	Initial biomass (g)	Final biomass (g)	Food uptake (g)	Food uptake/initial biomass	SGR (%)
1	2.71 ± 0.07	2.82 ± 0.02	0.74	0.27	0.2
2	2.92 ± 0.01	3.14 ± 0.03	0.71	0.24	0.4
3	2.64 ± 0.05	3.77 ± 0.02	1.75	0.66	1.8

coated nanoemulsions > chitosan-coated nanoemulsions. All nanosystems were stable for at least 18 days at 4 °C. The simplest nanosystem consisted of oily nanodroplets containing the pigment and stabilized by phospholipids (nanoemulsion) showing apparent hydrodynamic diameter of around 150 nm, and zeta potential ranging in time from around −60 to around −40 mV. These nanodroplets were coated with chitosan to afford chitosan-coated nanoemulsions. An optimal pH to prepare these formulations was found to be 3.5, and coated nanoemulsions of around 220 nm of hydrodynamic diameter and +70 mV of zeta potential were synthesized. The chitosan-coated nanoemulsions were converted into carrageenan-coated nanoemulsions by the addition of excess of carrageenan, achieving nanostructures of around 400 nm of hydrodynamic diameter and −50 mV of zeta potential. The photodegradation of AST included in the nanosystems, as well as free in acetone, followed a first order kinetics except in the case of the carrageenan-coated nanoemulsions. All these nanosystems could be incorporated in calcium alginate and chitosan tripolyphosphate beads of 2–3 mm. Macroscopic homogeneity was found in all formulations except for those containing alginate and chitosan-coated nanoemulsions. Photodegradation of the beads proceeded differently at naked eye, since color evanescence was observed for calcium alginate beads on its entire volume, whereas chitosan tripolyphosphate beads undergo discoloration from outside to inside. The discoloration kinetics of chitosan tripolyphosphate beads was independent on the nanosystem used to stabilize AST, related to the photosensitivity of chitosan. Calcium alginate beads of 2–3 mm containing AST have been supplied to zebrafish in a single dose in order to qualitatively demonstrate the attractiveness of the formulations, and calcium alginate microbeads of around 160 µm have been supplied to juvenile snook to confirm attractiveness and safety of the formulation.

Due to the easy preparation of the formulations (that exclude thermal treatment or the use of toxic solvents), and the flexibility of these hierarchically assembled materials to incorporate other active molecules (proteins, polyunsaturated fatty acids, oligoelements, oral vaccines, antibiotics, antiparasitic, etc.), hydrogels containing AST are ideal platforms to create foods for humans and animal species.

Supporting information description

Video S1 shows the consumption of alginate beads (2–3 mm of diameter) loaded with AST nanoemulsions by adult zebra fish.

Acknowledgments

This work was supported by FONDECYT Regular (Grant No.1120514, 1150899, 1161450, and 1181695) and FONDAP 15130011.

References

Aider, M. (2010). Chitosan application for active bio-based films production and potential in the food industry: Review. *Lebensmittel-Wissenschaft und -Technologie- Food Science and Technology, 43*(6), 837–842.
Alishahi, A., Mirvaghefi, A., Tehrani, M., Farahmand, H., Koshio, S., Dorkoosh, F., et al. (2011). Chitosan nanoparticle to carry vitamin C through the gastrointestinal tract and induce the non-specific immunity system of rainbow trout (Oncorhynchus mykiss). *Carbohydrate Polymers, 86*(1), 142–146.
Alishahi, A., Mirvaghefi, A., Tehrani, M., Farahmand, H., Shojaosadati, S., Dorkoosh, F., et al. (2011). Shelf life and delivery enhancement of vitamin C using chitosan nanoparticles. *Food Chemistry, 126*(3), 935–940.
Amar, E., Kiron, V., Satoh, S., & Watanabe, T. (2001). Influence of various dietary synthetic carotenoids on bio-defence mechanisms in rainbow trout, Oncorhynchus mykiss (Walbaum). *Aquaculture Research, 32*(s1), 162–173.
Ambati, R. R., Phang, S. M., Ravi, S., & Aswathanarayana, R. G. (2014). Astaxanthin: Sources, extraction, stability, biological activities and its commercial applications–a review. *Marine Drugs, 12*(1), 128–152.
Chávarri, M., Marañón, I., Ares, R., Ibáñez, F. C., Marzo, F., & del Carmen Villarán, M. (2010). Microencapsulation of a probiotic and prebiotic in alginate-chitosan capsules improves survival in simulated gastro-intestinal conditions. *International Journal of Food Microbiology, 142*(1), 185–189.
Christiansen, R., Lie, O., & Torrissen, O. J. (1995). Growth and survival of Atlantic salmon, Salmo salar L., fed different dietary levels of astaxanthin. First-feeding fry. *Aquaculture Nutrition, 1*(3), 189–198.
Flores, M. E., Garcés-Jerez, P., Fernández, D., Aros-Perez, G., González-Cabrera, D., Álvarez, E., et al. (2016). Facile formation of redox-active totally organic nanoparticles in water by in situ reduction of organic precursors stabilized through aromatic–aromatic interactions by aromatic polyelectrolytes. *Macromolecular Rapid Communications, 37*(21), 1729–1734.
Gammone, M., Riccioni, G., & D'Orazio, N. (2015). Marine carotenoids against oxidative Stress: Effects on human health. *Marine Drugs, 13*(10), 6226.
Gibbs, B. F., Kermasha, S., Alli, I., & Mulligan, C. N. (1999). Encapsulation in the food industry: A review. *International Journal of Food Sciences & Nutrition, 50*(3), 213–224.
Gouveia, L., & Empis, J. (2003). Relative stabilities of microalgal carotenoids in microalgal extracts, biomass and fish feed: Effect of storage conditions.

Innovative Food Science & Emerging Technologies, 4(2), 227–233.
Grenha, A., Gomes, M. E., Rodrigues, M., Santo, V. E., Mano, J. F., Neves, N. M., et al. (2010). Development of new chitosan/carrageenan nanoparticles for drug delivery applications. *Journal of Biomedical Materials Research Part A, 92*(4), 1265–1272.
Grimmig, B., Kim, S.-H., Nash, K., Bickford, P. C., & Douglas Shytle, R. (2017). Neuroprotective mechanisms of astaxanthin: A potential therapeutic role in preserving cognitive function in age and neurodegeneration. *GeroScience, 39*(1), 19–32.
Hassan, N., Oyarzun-Ampuero, F., Lara, P., Guerrero, S., Cabuil, V., Abou-Hassan, A., et al. (2014). Flow chemistry to control the synthesis of nano and microparticles for biomedical applications. *Current Topics in Medicinal Chemistry, 14*(5), 676–689.
Higuera-Ciapara, I., Felix-Valenzuela, L., & Goycoolea, F. (2006). Astaxanthin: A review of its chemistry and applications. *Critical Reviews in Food Science and Nutrition, 46*(2), 185–196.
Higuera-Ciapara, I., Felix-Valenzuela, L., Goycoolea, F., & Argüelles-Monal, W. (2004). Microencapsulation of astaxanthin in a chitosan matrix. *Carbohydrate Polymers, 56*(1), 41–45.
Kobayashi, M., Kakizono, T., Nishio, N., Nagai, S., Kurimura, Y., & Tsuji, Y. (1997). Antioxidant role of astaxanthin in the green alga Haematococcus pluvialis. *Applied Microbiology and Biotechnology, 48*(3), 351–356.
Kobayashi, M., & Sakamoto, Y. (1999). Singlet oxygen quenching ability of astaxanthin esters from the green alga Haematococcus pluvialis. *Biotechnology Letters, 21*(4), 265–269.
Krasaekoopt, W., Bhandari, B., & Deeth, H. C. (2006). Survival of probiotics encapsulated in chitosan-coated alginate beads in yoghurt from UHT-and conventionally treated milk during storage. *LWT-Food Science and Technology, 39*(2), 177–183.
Li, X., Kong, X., Shi, S., Zheng, X., Guo, G., Wei, Y., et al. (2008). Preparation of alginate coated chitosan microparticles for vaccine delivery. *BMC Biotechnology, 8*(1), 1.
McClements, D. J. (2013). Nanoemulsion-based oral delivery systems for lipophilic bioactive components: Nutraceuticals and pharmaceuticals. *Therapeutic Delivery, 4*(7), 841–857.
Naguib, Y. M. (2000). Antioxidant activities of astaxanthin and related carotenoids. *Journal of Agricultural and Food Chemistry, 48*(4), 1150–1154.
Nakano, T., Tosa, M., & Takeuchi, M. (1995). Improvement of biochemical features in fish health by red yeast and synthetic astaxanthin. *Journal of Agricultural and Food Chemistry, 43*(6), 1570–1573.
Nedovic, V., Kalusevic, A., Manojlovic, V., Levic, S., & Bugarski, B. (2011). An overview of encapsulation technologies for food applications. *Procedia Food Science, 1*, 1806–1815.
Orellana, S. L., Torres-Gallegos, C., Araya-Hermosilla, R., Oyarzun-Ampuero, F., & Moreno-Villoslada, I. (2015). Association efficiency of three ionic forms of oxytetracycline to cationic and anionic oil-in-water nanoemulsions analyzed by diafiltration. *Journal of Pharmaceutical Sciences, 104*(3), 1141–1152.
Oyarzun-Ampuero, F. A., Rivera-Rodríguez, G. R., Alonso, M. J., & Torres, D. (2013). Hyaluronan nanocapsules as a new vehicle for intracellular drug delivery. *European Journal of Pharmaceutical Sciences, 49*(4), 483–490.
Prabaharan, M. (2008). Review paper: Chitosan derivatives as promising materials for controlled drug delivery. *Journal of Biomaterials Applications, 23*(1), 5–36.
Rivas-Aravena, A., Sandino, A. M., & Spencer, E. (2013). Nanoparticles and microparticles of polymers and polysaccharides to administer fish vaccines. *Biological Research, 46*(4), 407–419.
Shahidi, F., & Han, X. Q. (1993). Encapsulation of food ingredients. *Critical Reviews in Food Science and Nutrition, 33*(6), 501–547.
Shah, M. M. R., Liang, Y., Cheng, J. J., & Daroch, M. (2016). Astaxanthin-producing green microalga haematococcus pluvialis: From single cell to high value commercial products. *Frontiers of Plant Science, 7*.
Sotomayor-Gerding, D., Oomah, B. D., Acevedo, F., Morales, E., Bustamante, M., Shene, C., et al. (2016). High carotenoid bioaccessibility through linseed oil nanoemulsions with enhanced physical and oxidative stability. *Food Chemistry, 199*, 463–470.
Sweeney, J. P., & Marsh, A. C. (1973). Liver storage of vitamin A in rats fed carotene stereoisomers. *Journal of Nutrition, 103*(1), 20–25.
Valenzuela, C., & Arias, J. I. (2012). Potenciales aplicaciones de películas de quitosano en alimentos de origen animal: Una revisión. *Avances en Ciencias Veterinarias, 27*(1).
Wasikiewicz, J. M., Yoshii, F., Nagasawa, N., Wach, R. A., & Mitomo, H. (2005). Degradation of chitosan and sodium alginate by gamma radiation, sonochemical and ultraviolet methods. *Radiation Physics and Chemistry, 73*(5), 287–295.
Whelehan, M., & Marison, I. W. (2011). Microencapsulation using vibrating technology. *Journal of Microencapsulation, 28*(8), 669–688.